Accepted Manuscript

On the performance of electrocatalytic anodes for photoelectro-Fenton treatment of synthetic solutions and real water spiked with the herbicide chloramben

Abdoulaye Thiam, Ignasi Sirés, Ricardo Salazar, Enric Brillas

PII:	S0301-4797(18)30823-5
DOI:	10.1016/j.jenvman.2018.07.065
Reference:	YJEMA 7786
To appear in:	*Journal of Environmental Management*
Received Date:	13 May 2018
Accepted Date:	18 July 2018

Please cite this article as: Abdoulaye Thiam, Ignasi Sirés, Ricardo Salazar, Enric Brillas, On the performance of electrocatalytic anodes for photoelectro-Fenton treatment of synthetic solutions and real water spiked with the herbicide chloramben, *Journal of Environmental Management* (2018), doi: 10.1016/j.jenvman.2018.07.065

TABLE OF CONTENTS

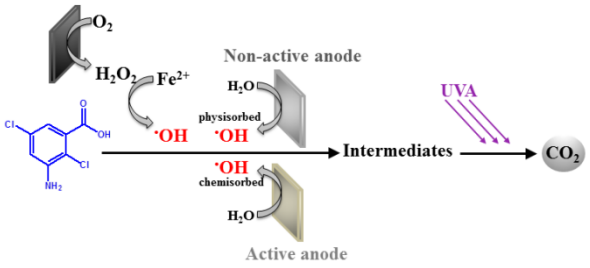

On the performance of electrocatalytic anodes for photoelectro-Fenton treatment of synthetic solutions and real water spiked with the herbicide chloramben

Abdoulaye Thiam,[a] Ignasi Sirés,*[b] Ricardo Salazar[c] and Enric Brillas*[b]

[a] *Programa Institucional de Fomento a la I+D+i, Universidad Tecnológica Metropolitana Ignacio Valdivieso 2409, P.O. Box 8940577, San Joaquín, Santiago, Chile*

[b] *Laboratori d'Electroquímica dels Materials i del Medi Ambient, Departament de Química Física, Universitat de Barcelona, Martí i Franquès 1-11, 08028 Barcelona, Spain.*

[c] *Laboratorio de Electroquímica del Medio Ambiente, LEQMA, Facultad de Química y Biología, Universidad de Santiago de Chile, USACh, Casilla 40, Correo 33, Santiago, Chile*

*Corresponding author: E-mail: i.sires@ub.edu (I. Sirés),

E-mail: brillas@ub.edu (E. Brillas)

Abstract

The destruction of the herbicide chloramben in 0.050 M Na_2SO_4 solutions at natural pH has been studied by photoelectro-Fenton with UVA light (PEF). The trials were carried out in a cell equipped with an air-diffusion cathode for H_2O_2 generation and different electrocatalytic anodes, namely active IrO_2-based and RuO_2-based electrodes and non-active boron-doped diamond (BDD) and PbO_2 ones. Similar removal rates were found regardless of the anode nature because the herbicide was mainly oxidized by $^{\bullet}OH$ formed from Fenton's reaction, which was enhanced by UVA-induced photo-Fenton reaction. The use of an IrO_2-based anode led to almost total mineralization at high current density, as also occurred with the powerful BDD anode, since photoactive intermediates originated from $^{\bullet}OH$-mediated oxidation were degraded under irradiation with UVA light. The good performance of the IrO_2-based anode in PEF was confirmed at different current densities and herbicide concentrations. The presence of Cl^- in the medium caused a slight deceleration of herbicide removal as well as mineralization inhibition, owing to the production of active chlorine with consequent formation of persistent chloroderivatives. Seven aromatic products along with oxalic and oxamic acids were identified in sulfate medium. Five aromatic derivatives were detected in Cl^--containing matrix, corroborating the generation of organochlorine compounds. In secondary effluent, larger mineralization was achieved by PEF with a BDD anode due to its high oxidation ability to destroy the chloroderivatives, although an acceptable performance was also obtained using an IrO_2-based anode.

Keywords: Chloramben; Dimensionally stable anode; Oxidation products; Photoelectro-Fenton; Urban wastewater

1. Introduction

The concern about water pollution by persistent organic pollutants is growing in parallel to the development of more efficient advanced oxidation processes (AOPs) for their destruction (Antonopoulou et al., 2014; Oturan and Aaron, 2014; Fernández-Castro et al., 2015; Johnson et al., 2017). Reactive oxygen species (ROS) such as hydroxyl radical (•OH) generated on site account for the high oxidation power of AOPs. With a standard potential E^o = 2.8 V/SCE, •OH is the second strongest oxidant known, being able to attack non-selectively most organics until overall mineralization is attained (Oturan and Aaron, 2014; Fernández-Castro et al., 2015). Fenton process, in which a mixture of Fe^{2+} and H_2O_2 originates homogeneous •OH in the bulk from the classical Fenton's reaction (1) with optimum pH near 3, is one of the most successful AOPs (Pignatello et al., 2006; Guinea et al., 2009; Ponnusami and Muthukumar, 2014; Matavos-Aramyan and Moussavi, 2017):

$$Fe2+ + H2O2 \rightarrow Fe3+ + \bullet OH + OH- \quad (1)$$

The poor Fe^{2+} regeneration from simultaneous Fenton-like reaction between Fe^{3+} and H_2O_2, the formation of Fe-rich sludge with loss of catalytic power, and the generation of refractory Fe(III)-carboxylate complexes are the main drawbacks of this method. These problems can be partially solved using the photo-Fenton process, where the solution is illuminated with UV light (Pignatello et al., 1999; Southworth and Voelker, 2003; Rahim Pouran et al., 2015; Seibert et al., 2017). The incident photons can photodecarboxylate the Fe(III) complexes according to general reaction (2), largely enhancing the mineralization process (Seibert et al., 2017). Additionally, a faster production of •OH is achieved from photoreduction of $Fe(OH)^{2+}$ species via reaction (3) (Pignatello et al., 1999; Southworth and Voelker, 2003).

$$Fe(COOR)2+ + h\nu \rightarrow Fe2+ + CO2 + R\bullet \quad (2)$$

$$Fe(OH)2+ + h\nu \rightarrow Fe2+ + \bullet OH \quad (3)$$

Alternative electrochemical AOPs (EAOPs) such as electro-Fenton (EF) and photoelectro-Fenton with UVA light (PEF) have been more recently developed (Brillas et al., 2009; Brillas, 2014; Sirés et al., 2014; Martínez-Huitle et al., 2015; Moreira et al., 2017). These processes show several advantages compared to non-electrochemical counterparts, like the use of smaller catalytic Fe^{2+} contents because regeneration is feasible from cathodic reduction of Fe^{3+} by reaction (4) (Dirany et al., 2012):

$$Fe3+ + e- \rightarrow Fe2+ \quad (4)$$

A key feature of Fenton-based electrochemical treatments is the continuous generation of H_2O_2 from cathodic O_2 reduction by reaction (5). Typical carbonaceous cathodes used for this are graphite felt (Vatanpour et al., 2009), carbon felt (Dirany et al., 2012; El-Ghenymy et al., 2014; Yahya et al., 2014; Dominguez et al., 2018), activated carbon fiber (Wang et al., 2008), carbon modified with metals (Assumpção et al., 2013), carbon nanotubes (Khataee et al., 2013, 2014), boron-doped diamond (BDD) (Cruz-González et al., 2010, 2012), and carbon-polytetrafluoroethylene (PTFE) employed in O_2- or air-diffusion devices (Salazar et al., 2012: Coria et al., 2016; Galia et al., 2016; Steter et al., 2018).

$$O2(g) + 2\,H+ + 2e- \rightarrow H2O2 \quad (5)$$

In an undivided cell, organic pollutants at pH 3 are destroyed by homogeneous $^{\bullet}OH$ formed from Fenton's reaction (1) in EF, along with that induced by photolytic reaction (3) in PEF. Moreover, organics can be attacked by heterogeneous M($^{\bullet}OH$) originated from water discharge at the anode M via reaction (6) at high current (Brillas et al., 2009; Sirés et al.,

2014). In the absence catalyst, the process is known as electrochemical oxidation with electrogenerated H_2O_2 (EO-H_2O_2) (Sirés et al., 2014; Martínez-Huitle et al., 2015).

$$M + H2O \rightarrow M(\bullet OH) + H+ + e- \quad (6)$$

Other oxidants can be produced depending on the dissolved salts. When the medium contains Cl^-, as occurs in natural water and industrial wastewater, this anion is anodically oxidized to active chlorine species (Cl_2/HClO) via reactions (7) and (8), which destroy the organic matter synergistically with hydroxyl radicals (Sirés et al., 2014; Martínez-Huitle et al., 2015: Moreira et al., 2017).

$$2Cl- \rightarrow Cl2(aq) + 2e- \quad (7)$$

$$Cl2(aq) + H2O \rightarrow HClO + Cl- + H+ \quad (8)$$

The oxidation power of EO-H_2O_2, EF and PEF also depends on the nature of the anode, which can behave as active or non active. In EO-H_2O_2, the best material in a non-chlorinated matrix is the non-active BDD electrode because it yields high quantities of BDD(•OH). This radical is more reactive than M(•OH) formed at active anodes like PbO_2 and dimensionally stable anodes (DSA®) due to the weaker adsorption (Sirés et al., 2014; Coria et al, 2016; Steter et al., 2016). In chlorinated media, however, IrO_2-based and RuO_2-based DSA® originate large amounts of active chlorine, which attacks the organic molecules in concomitance with M(•OH), yielding chloroderivatives that are highly stable against oxidation (Steter et al., 2016; Thiam et al., 2015, 2018). In earlier works, our group has reported the predominant role of UVA radiation as compared to the influence of the anode in PEF, due to the potential photodegradation of intermediates formed during the degradation of drugs (Coria et al., 2016), dyes (Thiam et al., 2015), chemicals (Steter et al., 2016, 2018) and

pesticides (Thiam et al., 2018). Nonetheless, more research is still required to provide sound conclusions on the viability of low cost DSA® in PEF regardless the reaction medium.

Chloramben (3-amino-2,5-dichlorobenzoic acid, $C_7H_5Cl_2NO_2$, M = 206.02 g mol^{-1}) is a pre-emergence herbicide used to control the seedlings of annual grasses and broadleaf weeds. It is highly soluble in water (near 700 mg L^{-1} at 25 ºC) and volatile, with tendency to contaminate groundwater. Chloramben has been detected in several U.S. states at 10 μg L^{-1} (Mir et al., 2012), being an irritant with moderate toxicity to honeybees and fishes. A reduced number of articles has reported the removal of chloramben either by photolysis in soils (Misra et al., 1997) and aqueous solutions (Bianco Prevot et al., 1999), or photocatalysis (Bianco Prevot et al., 1999; Mir et al., 2012). Using the latter AOP, total removal of 1.0 mM herbicide in a 250 mL solution with 30 mM H_2O_2 was achieved after 45 min of irradiation of TiO_2 with a 125 W UVC lamp, but with a decay < 20% of total organic carbon (TOC). Several by-products like 3-amino-5-chlorobenzoic, 2,5-dichlorobenzoic, chlorobenzoic and benzoic acids were detected by gas chromatography-mass spectrometry (GC-MS). However, there are no previous works on its destruction by EAOPs.

The aim of this article is to study the performance of PEF to degrade and mineralize chloramben solutions in order to show the viability of a DSA® electrode. The cell was an undivided tank reactor under UVA illumination, equipped with a carbon-PTFE air-diffusion cathode and a BDD, PbO_2, IrO_2-based or RuO_2-based anode. EO-H_2O_2 and EF trials were comparatively made to clarify the role of generated •OH and UVA light. The effect of current density and herbicide and chloride concentrations on PEF performance was examined. Aromatic intermediates and final carboxylic acids were identified by GC-MS and high-performance liquid chromatography (HPLC), respectively. The oxidation power of PEF with different anodes was finally assessed using urban wastewater spiked with chloramben, which

showed the influence of ionic composition and natural organic matter (NOM) on the herbicide mineralization.

2. Materials and methods

2.1. Chemicals

Chloramben (95% purity) was supplied by Sigma-Aldrich and used as received. Carboxylic acids were of analytical grade purchased from Panreac. The background electrolytes, Na_2SO_4 and NaCl, and $FeSO_4 \cdot 7H_2O$ used as catalyst source were of analytical grade from Fluka, Merck and Sigma-Aldrich, respectively. Other chemicals were either of analytical or HPLC grade supplied by Merck and Panreac. The synthetic solutions were prepared in ultrapure water (resistivity > 18.2 MΩ cm) from a Millipore Milli-Q system.

2.2. Real wastewater sample

Some electrolytic assays were carried out by spiking chloramben into urban wastewater. The fresh sample was collected from the secondary effluent of a wastewater treatment facility located in Gavà-Viladecans (Barcelona, Spain), preserved at 4 ºC and filtered before use. The characteristics of this sample were: pH = 7.9, specific conductivity = 3.2 mS cm^{-1}, total organic carbon (TOC) = 15.0 mg L^{-1}, along with 318.1 mg L^{-1} Cl^-, 141.3 mg L^{-1} SO_4^{2-}, 36.9 mg L^{-1} NH_4^+, 0.85 mg L^{-1} NO_3^-, 0.79 mg L^{-1} NO_2^-, and 0.19 mg L^{-1} Fe^{2+} as main ions.

2.3. Electrolytic systems

The electrolytic cell was a conventional undivided, cylindrical, double-jacketed tank reactor of 150 mL capacity. External thermostated water was recirculated through the double jacket to maintain the solution at 35 ºC, which ensured insignificant water evaporation. A solution volume of 100 mL was treated in each assay under vigorous stirring at 800 rpm with a magnetic bar. One of the following four electrodes was used as the anode in each trial: (i)

IrO_2-based plate (DSA®-O_2) purchased from NMT Electrodes, (ii) RuO_2-based plate (DSA®-Cl_2) purchased from NMT Electrodes, (iii) PbO_2 synthesized using the electrodeposition procedure described in earlier work (Sirés et al., 2009; Recio et al., 2011), and (iv) BDD thin-film over Si purchased from NeoCoat. In all tests, the cathode was a carbon-PTFE air-diffusion electrode purchased from E-TEK, mounted as described elsewhere (Steter et al., 2016), to generate H_2O_2 by pumping 1 L min^{-1} of air. The immersed area of each electrode was 3 cm^2 and the anode-cathode separation was 1 cm.

The EF and PEF treatments were carried out in the presence of 0.50 mM Fe^{2+}, since the catalyst concentration found as optimal for analogous studies with other organics was within the 0.5-1.0 mM range (Almeida et al., 2012; Lanzalaco et al., 2017**)**. The PEF experiments were run under irradiation of the solution with UVA light (365 nm) provided by a Philips TL/6W/08 fluorescent black light blue placed 5 cm above the solution (irradiance of 5 W m^{-2}). Galvanostatic trials were made by applying a constant current density (*j*) provided by an Amel 2049 potentiostat-galvanostat. Before the first assays, all the electrodes were electrochemically activated/cleaned under polarization in 0.050 M Na_2SO_4 at j = 100 mA cm^{-2} for 240 min.

2.4. Apparatus and analytical procedures

A Crison 2000 pH-meter was employed for pH measurement. Samples were withdrawn at regular time intervals from the treated solutions and microfiltered with 0.45 μm PTFE membrane filters from Whatman to be immediately analyzed.

The herbicide concentration was determined by reversed-phase HPLC using a Waters system composed of a 600 LC and a photodiode array detector set at λ = 297 nm. The LC was fitted with a BDS Hypersil C18 6 μm, 250 mm × 4.6 mm (i.d.), column at 35 °C. Prior to do this analysis, the samples were diluted with methanol to stop the degradation process. The aliquots were injected into the LC under circulation of a 60:40 (v/v) acetonitrile/water

(KH_2PO_4 10 mM, pH 3) mixture at 0.8 mL min^{-1}. The peak related to chloramben appeared in the chromatograms at retention time (t_r) of 4.6 min.

The solution TOC was determined on a Shimadzu VCSN TOC analyzer by injecting 50 μL samples. In this analysis, reproducible TOC values with ± 1% accuracy were found. From the TOC abatement (△TOC, mg L^{-1}) determined at time t (h) of a given experiment performed at current I (A), the mineralization current efficiency (MCE, %) was estimated by the following equation (Thiam et al., 2015):

$$\mathrm{MCE} = \frac{n\,F\,V\,(\Delta\mathrm{TOC})}{4.32\times10^{7} m\,I\,t}\times 100 \qquad (9)$$

where F is the Faraday constant (96,485 C mol^{-1}), V is the solution volume (L), 4.32×10^7 is a factor for units homogenization (3,600 s h^{-1} x 12,000 mg C mol^{-1}) and m = 7 is the number of carbon atoms of chloramben. An n-value of 24 was taken assuming the following total mineralization reaction of the herbicide to CO_2, with Cl^- and NH_4^+ as pre-eminent ions:

$$\mathrm{C7H5Cl2NO2} + 12\mathrm{H2O} \rightarrow 7\mathrm{CO2} + 2\mathrm{Cl}- + \mathrm{NH4}+ + 25\mathrm{H}+ + 24\mathrm{e}- \qquad (10)$$

The assays for assessing all decays were performed in triplicate, and average values are given along with the error bars corresponding to 95% confidence intervals in figures.

Primary aromatic intermediates formed at short electrolysis time of PEF treatments of 1.19 mM chloramben solutions in 0.50 M Na_2SO_4 and 0.011 M NaCl + 0.0015 M Na_2SO_4 at natural pH 3.42 and j = 33.3 mA cm^{-2} were detected by GC-MS. A non-polar Agilent J&W HP-5ms 0.25 μm, 30 m × 0.25 mm (i.d.), column was utilized and NIST05 MS library was used to correlate the mass spectra (Thiam et al., 2018). The generated short-linear aliphatic carboxylic acids were identified and quantified by ion-exclusion HPLC. The above LC fitted with a Bio-Rad Aminex HPX 87H, 300 mm × 7.8 mm (i.d), column at 35 °C was used,

following the procedure reported in an earlier work (Thiam et al., 2018). These chromatograms presented well-defined peaks related to oxalic (t_r = 6.9 min) and oxamic (t_r = 9.5 min) acids.

3. Results and discussion

3.1. Influence of the anode on the PEF treatment of chloramben in sulfate medium

A first series of assays was carried out to assess the importance of the anode in PEF process, using either BDD, PbO_2, IrO_2-based or RuO_2-based materials. The experiments were performed with 100 mL of a 1.19 mM herbicide solution (corresponding to 100 mg L^{-1} TOC) containing 0.050 M Na_2SO_4 and 0.50 mM Fe^{2+} as catalyst, by applying a j = 100 mA cm^{-2} for 300 min. The natural pH of the solution (3.42) was not modified, and it only showed a slight decay down to near 3, probably as a result of the formation of acidic by-products (Brillas et al., 2009; Sirés et al., 2014).

The abatement of the herbicide concentration in these trials is presented in Fig. 1a. A fast decay can be observed, achieving total removal in about 15 min, with analogous profiles for all the anodes tested. The exponential concentration decays were analyzed considering kinetic equations related to simple reaction orders, yielding best-fit linear regressions for a pseudo-first-order kinetics (see inset of Fig. 1a). From these correlations, a pseudo-first-order rate constant (k_1) of 0.47±0.02 min^{-1}, with a squared regression coefficient (R^2) close to 0.995, was determined regardless of the anode nature. These findings suggest that the pre-eminent oxidizing species reacting with chloramben is •OH generated from Fenton's reaction (1) and enhanced upon occurrence of reaction (3), with minor participation of M(•OH) formed at each anode surface from reaction (6). A small and constant quantity of •OH is then expected to be originated, which accounts for the pseudo-first-order behavior.

More significant influence of the anode material on PEF performance was found from the TOC removal of the same chloramben solutions. Fig. 1b reveals that the BDD anode allowed a slightly faster mineralization than the PbO_2 and IrO_2-based ones, at least during the first 120 min of electrolysis, although a similar mineralization with 95%-96% TOC abatement was achieved with these three anodes at 300 min. In contrast, the use of a RuO_2-based anode caused a deceleration of mineralization, with 82% TOC removal at 120 min, whereupon the decrease was practically inhibited until a final TOC reduction of 85% was attained (see Fig. 1b). The initially greater mineralization power of BDD as compared to PbO_2 and IrO_2-based anodes agrees with the gradually lower oxidation ability of generated M(•OH) in the sequence: BDD(•OH) > PbO_2(•OH) ~ IrO_2(•OH) > RuO_2(•OH) (Martínez-Huitle et al., 2015; Coria et al., 2016; Steter et al., 2018). Nevertheless, our results point to consider that the main oxidant was •OH in the bulk, as also reported for other compounds (Liu et al., 2017, 2018), which acted synergistically with UVA light that promoted the photodegradation of photoactive intermediates. At the end of these experiments, a NH_4^+ concentration of 0.70±0.05 mM was accumulated in the resulting solutions, related to 59±4% of the initial N content. Neither nitrate nor nitrite were detected, which means that the $–NH_2$ group of chloramben was pre-eminently mineralized to NH_4^+ ion, as proposed in reaction (10). The fact that the content of this ion did not account for all the initial N suggests the loss of volatile *N*-containing products such as N_2 and N_xO_y, as proposed for the treatment of other *N*-aromatics by EAOPs (Almeida et al., 2012; Salazar et al., 2012; Thiam et al., 2015, 2018).

From the above results, the MCE values for each experiment were calculated from Eq. (9), as depicted in the inset of Fig. 1b. As can be seen, greater MCE values of about 21%-22% were initially determined in PEF with the non-active BDD and PbO_2 anodes, meaning that a slightly faster mineralization occurred due to the action of BDD(•OH) and PbO_2(•OH). At longer time, when the mineralization was rather controlled by •OH and UVA radiation, quite

similar decay profiles can be observed in all cases, reaching low final values between 4% and 5%. The continuous fall of MCE can be accounted for by the formation of more persistent intermediates along with the gradual loss of organic matter (Sirés et al., 2014; Martínez-Huitle et al., 2015).

Based on the similar PEF results obtained using the active IrO_2-based anode and non-active BDD and PbO_2 ones, subsequent experiments were performed with the former anode in order to clarify its viability by examining the role of the oxidizing species and the effect of experimental variables and ions content in the aqueous matrix.

3.2. Comparative destruction of chloramben by EAOPs with an IrO_2-based anode

Fig. 2a shows a very slow abatement of the herbicide concentration during the EO-H_2O_2 treatment of 100 mL of a solution with 1.19 mM chloramben and 0.050 M Na_2SO_4 at natural pH and j = 100 mA cm^{-2}, only being reduced by 68% after 360 min. In contrast, the comparable EF and PEF processes in the presence of 0.50 mM Fe^{2+} yielded total removal at 20 and 15 min, respectively. This is an evidence of the very slow degradation of the herbicide with IrO_2($^{\bullet}$OH), the main oxidant in EO-H_2O_2, whereas it is very rapidly destroyed by $^{\bullet}$OH formed from Fenton's reaction (1) in EF. The decay is further accelerated in PEF due to the quicker Fe^{2+} regeneration from reaction (3). Note that no kinetic equation fitted the concentration decay during the EO-H_2O_2 treatment, suggesting a complex reaction between the herbicide and IrO_2($^{\bullet}$OH). A pseudo-first-order kinetics, however, was obeyed in EF and PEF, with k_1-values of 0.35 min^{-1} (R^2 = 9.996) and 0.44 min^{-1} (R^2 = 0.994), respectively.

This behavior was also confirmed from the corresponding TOC removal as depicted in Fig. 2b. A growing oxidation power of the EAOPs can be observed in the sequence: EO-H_2O_2 < EF < PEF. The very low oxidation ability of IrO_2($^{\bullet}$OH) and generated H_2O_2 only allowed a poor TOC abatement of 9% at 300 min of EO-H_2O_2. The EF process was much more powerful and 55% TOC removal was achieved at the end. This means that the $^{\bullet}$OH amount

coming from Fenton's reaction (3) was enough to mineralize many intermediates in the bulk, although a large proportion of by-products could not be removed by this radical. In contrast, the PEF treatment led to 96% TOC reduction and hence, almost total mineralization is feasible because the incident UVA photons photodegrade those by-products that cannot be destroyed by •OH. This explains the low influence of the anode in the PEF treatment of chloramben.

3.3. Effect of experimental parameters and chloride concentration on PEF process

First, the influence of j between 33.3 and 100 mA cm^{-2} on the performance of PEF treatment of 1.19 mM herbicide in sulfate medium with 0.50 mM Fe^{2+} at natural pH was assessed using the IrO_2-based/air-diffusion cell. Fig. 3a highlights a very rapid decay of chloramben concentration in all cases, disappearing after 40 min at 33.3 mA cm^{-2} and 15 min at 100 mA cm^{-2}. The enhancement of herbicide removal with raising j can be associated with the concomitant faster generation of •OH (along with M(•OH)). This is feasible because greater H_2O_2 concentration is produced from reaction (5) at higher j, which then reacts more rapidly with Fe^{2+} to accelerate •OH generation from Fenton's reaction (1) (Brillas et al., 2009; Almeida et al., 2012). From the pseudo-first-order linear correlations shown in the inset, increasing k_1-values of 0.16 min^{-1} (R^2 = 0.990), 0.33 min^{-1} (R^2 = 0.995) and 0.44 min^{-1} (R^2 = 0.994) were determined for 33.3, 66.7 and 100 mA cm^{-2}, respectively. This evidences a constant •OH production for all the j values.

Conversely, much smaller differences in TOC decay were found in these trials. Fig. 3b shows a slightly slower mineralization at j = 33.3 mA cm^{-2} up to 120 min of electrolysis, whereupon TOC reduction was practically inhibited and finally attained 88%. Similar abatements can be observed at 66.7 and 100 mA cm^{-2} up to approximately 120 min, where TOC was reduced by 86% and 89%, respectively. Further TOC decays, however, were much poorer, eventually reaching 90% and 96%. The quick loss of TOC during the first 120 min of

PEF treatment at all *j* tested is due to the fast photolysis of intermediates under UVA irradiation. The predominant role of UVA light minimizes the greater oxidation rate resulting from increase of *j*. At longer time, all photoactive intermediates seem to be already mineralized, and the remaining by-products are very slowly destroyed because they are quite stable against hydroxyl radicals. In PEF, a loss in MCE is expected at higher *j* since a larger proportion of •OH in the bulk is consumed by parasitic non-oxidizing reactions, like its dimerization and its attack over H_2O_2 (Brillas, 2014; Martínez-Huitle et al., 2015). This behavior can be confirmed in the inset of Fig. 3b at long electrolysis time, with decreasing final MCE values of 13.5%, 6.9% and 4.9% at raising *j* of 33.3, 66.7 and 100 mA cm^{-2}. These results inform about the convenience of using low *j* values, in order to operate with lower energy consumptions.

The influence of the herbicide concentration on PEF process was studied under the same conditions by applying the lowest *j* = 33.3 mA cm^{-2} to better elucidate the role of oxidizing agents. As can be seen in Fig. 4a, the normalized concentration decay was progressively decelerated as the herbicide content rose from 0.59 to 2.38 mM, disappearing at 30 and 120 min of the treatment, respectively. This trend seems logical because analogous quantities of hydroxyl radicals were originated in these trials at a fixed *j*. This leads to a slower slope of the straight lines accounting for a pseudo-first-order kinetics (see the inset of Fig. 4a), with decreasing k_1-values of 0.21 min^{-1} (R^2 = 0.987), 0.16 min^{-1} (R^2 = 0.990) and 0.062 min^{-1} (R^2 = 0.998) at 0.59, 1.19 and 2.38 mM chloramben, respectively. Hence, the herbicide abatement did not follow a true pseudo-first-order reaction, meaning that under each experimental condition a different steady •OH concentration is formed.

Regarding the corresponding TOC removals, an S-shape profile was obtained at the highest herbicide content. In this case, Fig. 4b shows a slow mineralization up to 120 min, followed by a very fast TOC decay until the end of the trial. This behavior suggests a gradual

generation of photoactive intermediates from •OH oxidation, which are very effectively photodegraded by UVA light between 120 and 300 min. In contrast, a progressive TOC abatement can be observed in Fig. 4b starting at 1.19 and 0.59 mM, suggesting a quicker formation of photoactive organics that are then rapidly photodegraded. TOC removal was 88-90% at the end of all these trials, regardless the initial herbicide content, which can be explained by the production of a similar proportion of persistent by-products (10-12% of the initial C) to oxidation/photolysis. The MCE values in these assays agree with the TOC profiles. The inset of Fig. 4b highlights maximum MCE values of 29.3% at 40 min, 35.1% at 90 min and 31.3% at 240 min at 0.59, 1.19 and 2.38 mM, respectively. This corresponds to the transition between increasing and decreasing mineralization rates, the latter being due to the progressive loss of organic matter and the larger accumulation of refractory by-products. The shift of the maximal to longer time with increasing herbicide content confirms the slower generation of photoactive by-products, as stated above. Note that, when treating highly concentrated solutions, the MCE values may rose at long time (e.g., 180 min), suggesting a larger availability of •OH that arises from the deceleration of its parasitic reactions (Brillas et al., 2009; Brillas, 2014; Sirés et al., 2014; Martínez-Huitle et al., 2015).

Since urban and industrial wastewater usually contain a large amount of Cl^- ion, apart from SO_4^{2-} ion, the effect of the former ion on PEF treatment of 1.19 mM chloramben solutions at natural pH was investigated at j = 33.3 mA cm^{-2}. Fig. 5a reveals that using 0.035 M NaCl + 0.025 M Na_2SO_4 (same conductivity as 0.050 M Na_2SO_4, i.e., 5.8 mS cm^{-1}) and 0.011 M NaCl + 0.0015 M Na_2SO_4 (similar conductivity, near 3 mS cm^{-1}, as compared to real wastewater) as synthetic aqueous matrices, complete removal of the herbicide was reached after 40 min, the same time needed with 0.050 M Na_2SO_4. Nevertheless, a slower decay occurred with 0.035 M NaCl, which was more significant when the Cl^- content dropped to 0.011 M. In these media, the production of high amounts of active chlorine (Cl_2/HClO) from

Cl^- oxidation at the IrO_2-based anode by reactions (7) and (8) is expected (Coria et al., 2016; Steter et al., 2016). The profiles of Fig. 5a suggest a competition between both, active chlorine and •OH, to attack the herbicide in the bulk. The corresponding k_1-values determined from the linear regressions shown in the inset panel of Fig. 5a rose from 0.12 min^{-1} (R^2 = 0.989) in the presence of 0.011 M NaCl to 0.14 min^{-1} (R^2 = 0.993) using 0.035 M NaCl, a value slightly smaller than 0.16 min^{-1} found in the Cl^--free medium. The fact that a pseudo-first-order kinetics was always found means that a steady concentration of all oxidizing agents was always formed. As presented in Fig. 5b, the TOC decays determined during these experiments were quite similar up to 60 min of electrolysis, reaching about 40% mineralization. At longer time, smaller amounts of TOC were removed as the solution contained more Cl^-. Thus, TOC was reduced by 88% in 0.050 M Na_2SO_4, 82% in the solution with 0.011 M NaCl and 72% in that with 0.035 M NaCl. This is also confirmed from the 13.5%, 12.5% and 10.9% MCE values finally reached (see inset of Fig. 5b). This tendency can be accounted for the fast photodegradation of non-chlorinated photoactive products in the two latter matrices, with larger formation of persistent chloroderivatives as the medium contains more Cl^-. Consequently, the presence of excessively high concentrations of the latter ion may become detrimental for chloramben mineralization.

3.4. Identification of aromatic intermediates and final carboxylic acids

Fig. 6 shows a general reaction sequence for the primary degradation of chloramben. It includes the aromatic products detected by GC-MS when 1.19 mM chloramben solutions in 0.050 M Na_2SO_4 or 0.011 M NaCl + 0.0015 M Na_2SO_4 were treated for short times under PEF conditions with an IrO_2-based/air-diffusion cell at j = 33.3 mA cm^{-2}. This pathway presupposes than in sulfate medium, the main oxidizing agent is •OH in the bulk, whereas in chlorinated matrix, active chlorine (Cl_2/HClO) acts synergistically.

Upon •OH-mediated oxidation in 0.050 M Na_2SO_4, chloramben was decarboxylated to yield 2,5-dichlorobenzamine, deaminated to 2,5-dichlorobenzoic acid and dechlorinated to 3-amino-5-chlorobenzoic acid. The former compound was further hydroxylated to 3-amino-2,5-dichlorophenol, which was subsequently deaminated to 2,5-dichloro-1,3-benzenediol. The other two compounds were in turn either dechlorinated or deaminated to yield 3-chlorobenzoic acid, followed by dechlorination to form benzoic acid. It is noteworthy that 3-amino-5-chlorobenzoic, 2,5-dichlorobenzoic and benzoic acids have also been reported as by-products during the degradation of chloramben by TiO_2/H_2O_2/UVC (Bianco Prevot et al., 1999).

In the presence of chloride, the oxidation with •OH yielded 2,5-dichlorobenzamine, which was deaminated and hydroxylated to 2,5-dichloro-1,3-benzenediol. Fig. 6 highlights the consecutive chlorination of the latter compound with active chlorine leading to 2,4,5-trichloro-1,3-benzenediol and 2,3,4,5-tetrachlorophenol. On the other hand, direct chlorination + hydroxylation of chloramben yielded 3,5,6-trichlorosalicylic acid with loss of NH_4^+ ion. The detection of these intermediates corroborates the generation of persistent chloroderivatives that inhibit the total mineralization of the herbicide in chlorinated matrices.

Further evolution of the above aromatic intermediates involves the cleavage of the benzene moiety with the expected formation of final short-linear aliphatic carboxylic acids (Almeida et al., 2012; Thiam et al., 2015, 2018; Steter et al., 2016, 2018). This was confirmed for chloramben by analyzing the 1.19 mM solutions treated under the EF and PEF conditions described in Fig. 2. Two final acids, oxalic and oxamic, which are directly mineralized to CO_2, were detected. Fig. 7a highlights that oxalic acid was accumulated up to 111 mg L^{-1} after 60-90 min of EF, whereupon its content remained stable. The refractory Fe(III)-oxalate complexes formed in the bulk allow explaining this behavior (Almeida et al., 2012). The fast photodecarboxylation of these complexes under UVA light irradiation via reaction (2)

justifies its disappearance after 120-180 min of PEF (see Fig. 7a). In the case of oxamic acid, Fig. 7b reveals the accumulation of 16-18 mg L^{-1} after 60-90 of EF, whereas in PEF, it drops from 10.4 mg L^{-1} at 120 min to 5.4 mg L^{-1} at 300 min, indicating a slower photolysis of its Fe(III) complexes. A mass balance at the end of these EF and PEF treatments shows that the content of both carboxylic acids corresponds to 33.90 and 1.45 mg L^{-1} of TOC, respectively, related to a 75.3% and 32.2% of the organic matter present in the treated solutions (see Fig. 2b). These results confirm that total mineralization is prevented by the formation of other by-products that are hard to degrade by •OH and UVA radiation. Moreover, the great amount of oxalic acid formed explains the high effectiveness of PEF, which allows the quick photodegradation of its Fe(III) complexes, not being feasible in EF.

3.5. PEF treatment of chloramben spiked into urban wastewater

The study of the PEF treatment of chloramben was extended to urban wastewater as reaction matrix, which contains Cl^- and SO_4^{2-} ions as well as NOM (mainly composed by humic and fulvic acids). Preliminary treatment of raw wastewater conditioned at pH 3.4, in the presence of 0.50 mM Fe^{2+}, using a BDD or IrO_2-based anode at j = 33.3 mA cm^{-2} showed total removal of initial TOC (15 mg L^{-1}) in 300 min.

Fig. 8a presents the similar decay found from 1.19 mM herbicide spiked into urban wastewater under the above conditions using a BDD or IrO_2-based anode. It disappeared in 40 min, i.e., the same time as that required in 0.050 M Na_2SO_4 and chlorinated matrices (see Fig. 5a). The inset panel shows the good fit to pseudo-first-order kinetics determined for the concentration decay, yielding the same k_1-value of 0.13 min^{-1} with R^2 = 0.995 for each anode. This is slightly lower than 0.14-0.16 min^{-1} obtained in 0.050 M Na_2SO_4 and 0.035 M NaCl + 0.025 M Na_2SO_4, meaning that •OH and active chlorine are partially consumed by NOM in urban wastewater.

Fig. 8b evidences a similar decay rate of the initial TOC (115 mg L^{-1}) regardless of the anode used, attaining 60% abatement during the first 90 min of PEF treatment. At longer time, TOC dropped slowly with 74% reduction using an IrO_2-based anode and much rapidly (82% decay) with BDD up to about 180 min, whereupon it remained practically constant. The final TOC in the former case was 30 mg L^{-1}, a value quite analogous to 28 mg L^{-1} remaining after the treatment in 0.035 M NaCl + 0.025 M Na_2SO_4 (see Fig. 5b). This can be related to a large formation of stable chloroderivatives, probably coming from the reaction of oxidation products or some components of NOM, which are responsible for the partial mineralization. The superior oxidation power of BDD can be ascribed to the partial removal of such persistent by-products with the powerful BDD(•OH). Nevertheless, the IrO_2-based anode is an excellent alternative to destroy most by-products of chloramben in urban wastewater by PEF. Note that the present PEF results are better than 64% TOC removal reported in earlier work considering a similar treatment of 50 mg L^{-1} of TOC of pesticide carbofuran spiked into urban wastewater with a RuO_2-based/air-diffusion cell at j = 50 mA cm^{-2} (Thiam et al., 2018).

4. Conclusions

It has been shown that chloramben is degraded at similar rate either in synthetic media with sulfate and/or chloride ions, or urban wastewater, at pH near 3. Overall, the anode nature played a minor role. This is related to the pre-eminent degradation by •OH formed in the bulk and UVA irradiation. The presence of Cl^- decelerated the herbicide removal because of its slower reaction with active chlorine. The viability of an IrO_2-based DSA® in PEF was confirmed from the 96% TOC reduction achieved in 0.050 M Na_2SO_4. This large mineralization was obtained thanks to the formation of photoactive intermediates, like Fe(III)-carboxylate complexes, upon •OH attack, being further photograded by UVA light. The generation of persistent chloroderivatives in chlorinated media inhibited the mineralization

process. These by-products were more effectively destroyed by BDD in urban wastewater, although an acceptable performance was obtained with the IrO_2-based anode. A general pathway for the herbicide mineralization has been proposed from the aromatics identified in the presence of sulfate and chloride.

Acknowledgements

The authors acknowledge financial support from project CTQ2016-78616-R (AEI/FEDER, EU) and FONDECYT project 3160753 (CONICYT, Chile).

References

Almeida, L.C., Garcia-Segura, S., Arias, C., Bocchi, N., Brillas, E., 2012. Electrochemical mineralization of the azo dye Acid Red 29 (Chromotrope 2R) by photoelectro-Fenton process. Chemosphere 89, 751-758.

Antonopoulou, M., Evgenidou, E., Lambropoulou, D., Konstantinou, I., 2014. A review on advanced oxidation processes for the removal of taste and odor compounds from aqueous media. Water Res. 53, 215-234.

Assumpção, M.H.M.T., Moraes, A., De Souza, R.F.B., Reis, R.M., Rocha, R.M., Gaubeur, I., Calegaro, M.L., Hammer, P., Lanza, M.R.V., Santos, M.C., 2013. Degradation of dipyrone via advanced oxidation processes using a cerium nanostructured electrocatalyst material. Appl. Catal. A: Gen. 462-463, 256-261.

Bianco Prevot, A., Vincenti, M., Bianciotto, A., Pramauro, E., 1999. Photocatalytic and photolytic transformation of chloramben in aqueous solutions. Appl. Catal. B: Environ. 22, 149-158.

Brillas, E., 2014. A review on the degradation of organic pollutants in waters by UV photoelectro-Fenton and solar photoelectro-Fenton. J. Braz. Chem. Soc. 25, 393-417.

Brillas, E., Sirés, I., Oturan, M.A., 2009. Electro-Fenton process and related electrochemical technologies based on Fenton's reaction chemistry. Chem. Rev. 109, 6570-6631.

Coria, G., Sirés, I., Brillas, E., Nava, J.L., 2016. Influence of the anode material on the degradation of naproxen by Fenton-based electrochemical processes. Chem. Eng. J. 304, 817-825.

Cruz-González, K., Torres-López, O., García-León, A., Brillas, E., Hernández-Ramírez, A., Peralta-Hernández, J.M., 2012. Optimization of electro-Fenton/BDD process for decolorization of a model azo dye wastewater by means of response surface methodology. Desalination 286, 63-68.

Cruz-González, K., Torres-López, O., García-León, A., Guzmán-Mar, J.L., Reyes, L.H., Hernández-Ramírez, A., Peralta-Hernández, J.M., 2010. Determination of optimum operating parameters for Acid Yellow 36 decolorization by electro-Fenton process using BDD cathode. Chem. Eng. J. 160, 199-206.

Dirany, A., Sirés, I., Oturan, N., Özcan, A., Oturan, M.A., 2012. Electrochemical treatment of the antibiotic sulfachloropyridazine: Kinetics, reaction pathways, and toxicity evolution. Environ. Sci. Technol. 46, 4074-4082.

Dominguez, C.M., Oturan, N., Romero, A., Santos, A., Oturan, M.A., 2018. Optimization of electro-Fenton process for effective degradation of organochlorine pesticide lindane. Catal. Today, https://doi.org/10.1016/j.cattod.2017.10.028

El-Ghenymy, A., Rodríguez, R.M., Brillas, E., Oturan, N., Oturan, M.A., 2014. Electro-Fenton degradation of the antibiotic sulfanilamide with Pt/carbon-felt and BDD/carbon-felt cells. Kinetics, reaction intermediates, and toxicity assessment. Environ. Sci. Pollut. Res. 21, 8368-8378.

Fernández-Castro, P., Vallejo, M., San Román, M.F., Ortiz, I., 2015. Insight on the fundamentals of advanced oxidation processes. Role and review of the determination methods of reactive oxygen species. J. Chem. Technol. Biotechnol. 90, 796-820.

Galia, A., Lanzalaco, S., Sabatino, M.A., Dispenza, C., Scialdone, O., Sirés, I., 2016. Crosslinking of poly(vinylpyrrolidone) activated by electrogenerated hydroxyl radicals: A first step towards a simple and cheap synthetic route of nanogel vectors. Electrochem. Commun. 62, 64-68.

Guinea, E., Brillas, E., Centellas, F., Cañizares, P., Rodrigo, M.A., Sáez, C., 2009. Oxidation of enrofloxacin with conductive-diamond electrochemical oxidation, ozonation and Fenton oxidation. A comparison. Water Res. 43, 2131-2138.

Johnson, G.J., Bullen, L.A., bin Mohd Akil, M.R., 2017. Review on emerging pollutants and advanced oxidation processes. Int. J. Adv. Res. 5, 2315-2324.

Khataee, A., Akbarpour, A., Vahi, B., 2014. Photoassisted electrochemical degradation of an azo dye using Ti/RuO_2 anode and carbon nanotubes containing gas-diffusion cathode. J. Taiwan Inst. Chem. Eng. 45, 930-936.

Khataee, A., Khataee, A., Fathinia, M., Vahid, B., Joo, S.W., 2013. Kinetic modeling of photoassisted-electrochemical process for degradation of an azo dye using boron-doped diamond anode and cathode with carbon nanotubes. J. Ind. Eng. Chem. 19, 1890-1894.

Lanzalaco, S., Sirés, I., Sabatino, M.A.. Dispenza, C. Scialdone, O., Galia, A., 2017. Synthesis of polymer nanogels by electro-Fenton process: investigation of the effect of main operation parameters. Electrochim. Acta 246, 812-822.

Liu, X., Yang, D., Zhou, Y., Zhang, J., Luo, L., Meng, S., Chen, S., Tan, M., Li, Z., Tang, L., 2017. Electrocatalytic properties of N-doped graphite felt in electro-Fenton process and degradation mechanism of levofloxacin. Chemosphere 182, 306-315.

Liu, X., Zhou, Y., Zhan, J., Luo, L., Yang, Y., Huang, H., Peng, H., Tang, L., Mu, Y., 2018. Insight into electro-Fenton and photo-Fenton for the degradation of antibiotics: mechanism study and research gaps. Chem. Eng. J. 347, 379-397.

Martínez-Huitle, C.A., Rodrigo, M.A., Sirés, I., Scialdone, O., 2015. Single and coupled electrochemical processes and reactors for the abatement of organic water pollutants: A critical review. Chem. Rev. 115, 13362-13407.

Matavos-Aramyan, S., Moussavi, M., 2017. Advances in Fenton and Fenton based oxidation processes for industrial effluent contaminants control-A review. Int. J. Environ. Sci. Nat. Res. 2, 555594.

Mir, N.A., Haque, M.M., Khan, A., Umar, K., Muneer, M., Vijayalakshmi, S., 2012. Semiconductor mediated photocatalysed reaction of two selected organic compounds in aqueous suspensions of titanium dioxide. J. Adv. Oxid. Technol. 15, 380-391.

Misra, B., Graebing, P.W., Chib, J.S., 1997. Photodegradation of chloramben on a soil surface: A laboratory-controlled study. J. Agric. Food Chem. 45, 1464-1467.

Moreira, F.C., Boaventura, R.A.R., Brillas, E., Vilar, V.J.P., 2017. Electrochemical advanced oxidation processes: A review on their application to synthetic and real wastewaters. Appl. Catal. B: Environ. 202, 217-261.

Oturan, M.A., Aaron, J.-J., 2014. Advanced oxidation processes in water/wastewater treatment: Principles and applications. A review. Crit. Rev. Environ. Sci. Technol. 44, 2577-2641.

Pignatello, J.J., Liu, D., Huston, P., 1999. Evidence for an additional oxidant in the photoassisted Fenton reaction. Environ. Sci. Technol. 33, 1832-1839.

Pignatello, J.J., Oliveros, E., MacKay, A., 2006. Advanced oxidation processes for organic contaminant destruction based on the Fenton reaction and related chemistry. Crit. Rev. Environ. Sci. Technol. 36, 1-84.

Ponnusami B., Muthukumar, K., 2014. A review on Fenton and improvements to the Fenton process for wastewater treatment. J. Environ. Chem. Eng. 2, 557-572.

Rahim Pouran, S., Abdul Aziz, A.R., Wan Daud, W.M.A., 2015. Review on the main advances in photo-Fenton oxidation system for recalcitrant wastewaters. J. Ind. Eng. Chem. 21, 53-69.

Recio, F.J., Herrasti, P., Sirés, I., Kulak, A.N., Bavykin, D.V., Ponce-de-León, C., Walsh, F.C., 2011. The preparation of PbO_2 coatings on reticulated vitreous carbon for the electro-oxidation of organic pollutants. Electrochim. Acta 56, 5158-5165.

Salazar, R., E. Brillas, E., Sirés, I., 2012. Finding the best Fe^{2+}/Cu^{2+} combination for the solar photoelectro-Fenton treatment of simulated wastewater containing the industrial textile dye Disperse Blue 3. Appl. Catal. B: Environ. 115–116, 107–116.

Seibert, D., Diel, T., Welter, J.B., de Souza, A.L., Módenes, A.N., Espinoza-Quiñones, F.R., Borba, F.H., 2017. Performance of photo-Fenton process mediated by Fe (III)-carboxylate complexes applied to degradation of landfill leachate. J. Environ. Chem. Eng. 5, 4462-4470.

Sirés, I., Brillas, E., Oturan, M.A., Rodrigo, M.A., Panizza, M., 2014. Electrochemical advanced oxidation processes: today and tomorrow. A review. Environ. Sci. Pollut. Res. 21, 8336-8367.

Sirés, I., Low, C.T.W., Ponce de Leon, C., Walsh, F.C., 2009. The deposition of nanostructured β-PbO_2 coatings from aqueous methanesulfonic acid for the electrochemical oxidation of organic pollutants. Electrochem. Commun. 12, 70-74.

Southworth, B.A., Voelker, B.M., 2003. Hydroxyl radical production via the photo-Fenton reaction in the presence of fulvic acid. Environ. Sci. Technol. 37, 1130-1136.

Steter, J.R., Brillas, E., Sirés, I., 2016. On the selection of the anode material for the electrochemical removal of methylparaben from different aqueous media. Electrochim. Acta 222, 1464-1474.

Steter, J.R., Brillas, E., Sirés, I., 2018. Solar photoelectro-Fenton treatment of a mixture of parabens spiked into secondary treated wastewater effluent at low input current. Appl. Catal. B: Environ. 224, 410-418.

Thiam, A., Salazar, R., Brillas, E., Sirés, I., 2018. Electrochemical advanced oxidation of carbofuran in aqueous sulfate and/or chloride media using a flow cell with a RuO_2-based anode and an air-diffusion cathode at pre-pilot scale. Chem. Eng. J. 335, 133-144.

Thiam, A., Sirés, I., Garrido, J.A., Rodríguez, R.M., E. Brillas, E., 2015. Effect of anions on electrochemical degradation of azo dye Carmoisine (Acid Red 14) using a BDD anode and air-diffusion cathode. Separ. Purif. Technol. 140, 43-52.

Vatanpour, V., Daneshvar, N., Rasoulifard, M.H., 2009. Electro-Fenton degradation of synthetic dye mixture: influence of intermediates. J. Environ. Eng. Manage. 19, 277-282.

Wang, A., Qu, J., Liu, H., Ru, J., 2008. Mineralization of an azo dye Acid Red 14 by photoelectro-Fenton process using an activated carbon fiber cathode. Appl. Catal. B: Environ. 84, 393-399.

Yahya, M.S., Oturan, N., El Kacemi, K., El Karbane, M., Aravindakumar, C.T., Oturan, M.A., 2014. Oxidative degradation study on antimicrobial agent ciprofloxacin by electro-Fenton process: Kinetics and oxidation products. Chemosphere 117, 447-454.

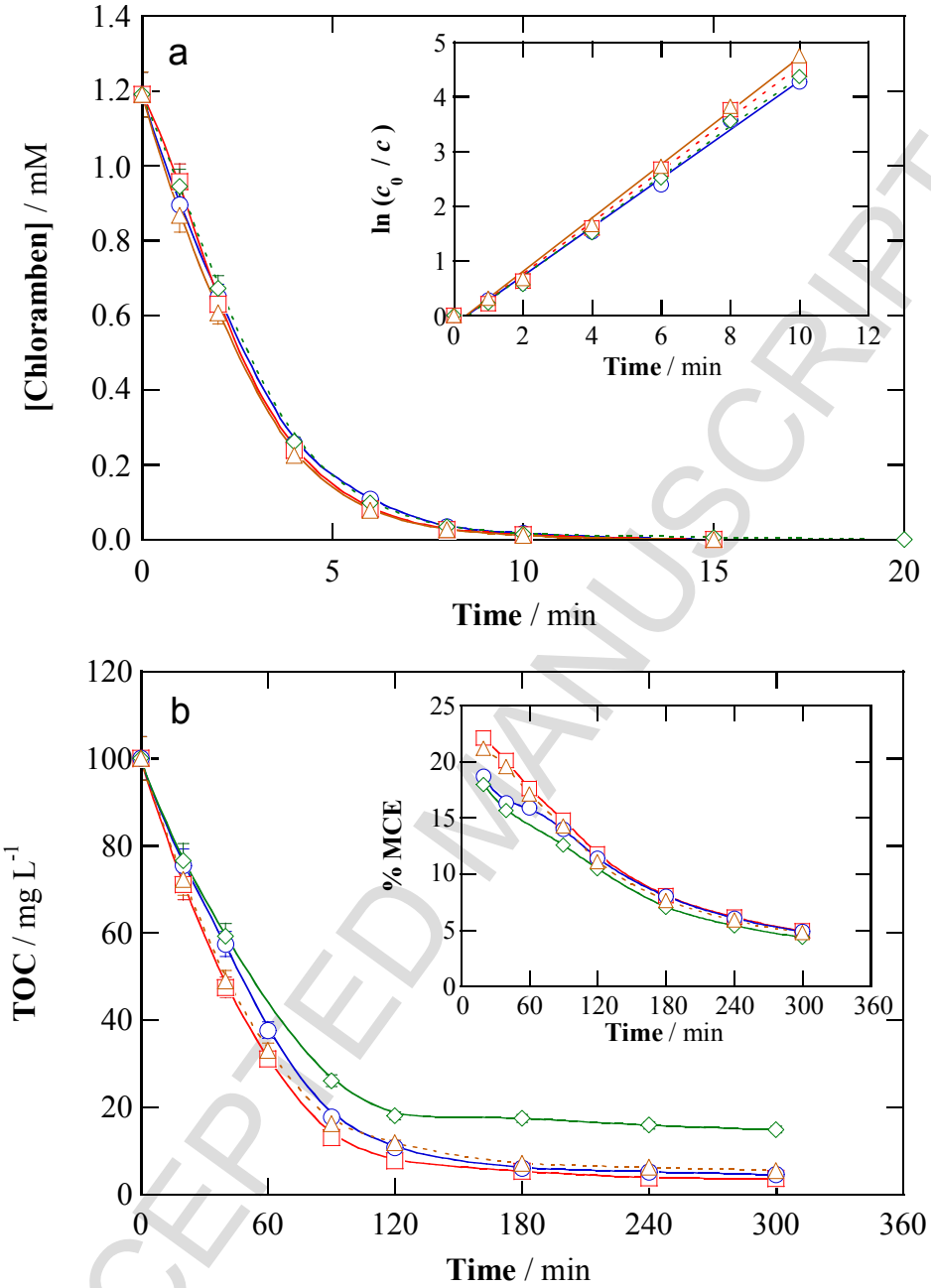

Fig. 1. Decay of (a) chloramben concentration and (b) TOC with electrolysis time for the PEF treatment of 100 mL of solutions with 1.19 mM herbicide, 0.050 M Na_2SO_4 and 0.50 mM Fe^{2+} at natural pH 3.42 using cells with an air-diffusion cathode (3 cm^2 electrodes area), operating at current density (j) of 100 mA cm^{-2}, 35 °C, under irradiation with a 6 W UVA (λ_{max} = 365 nm) lamp. Anode: (□) BBD, (△) PbO_2, (◇) RuO_2-based and (○) IrO_2-based. The kinetic analysis considering a pseudo-first-order reaction and the MCE values are presented in the inset panels of (a) and (b), respectively.

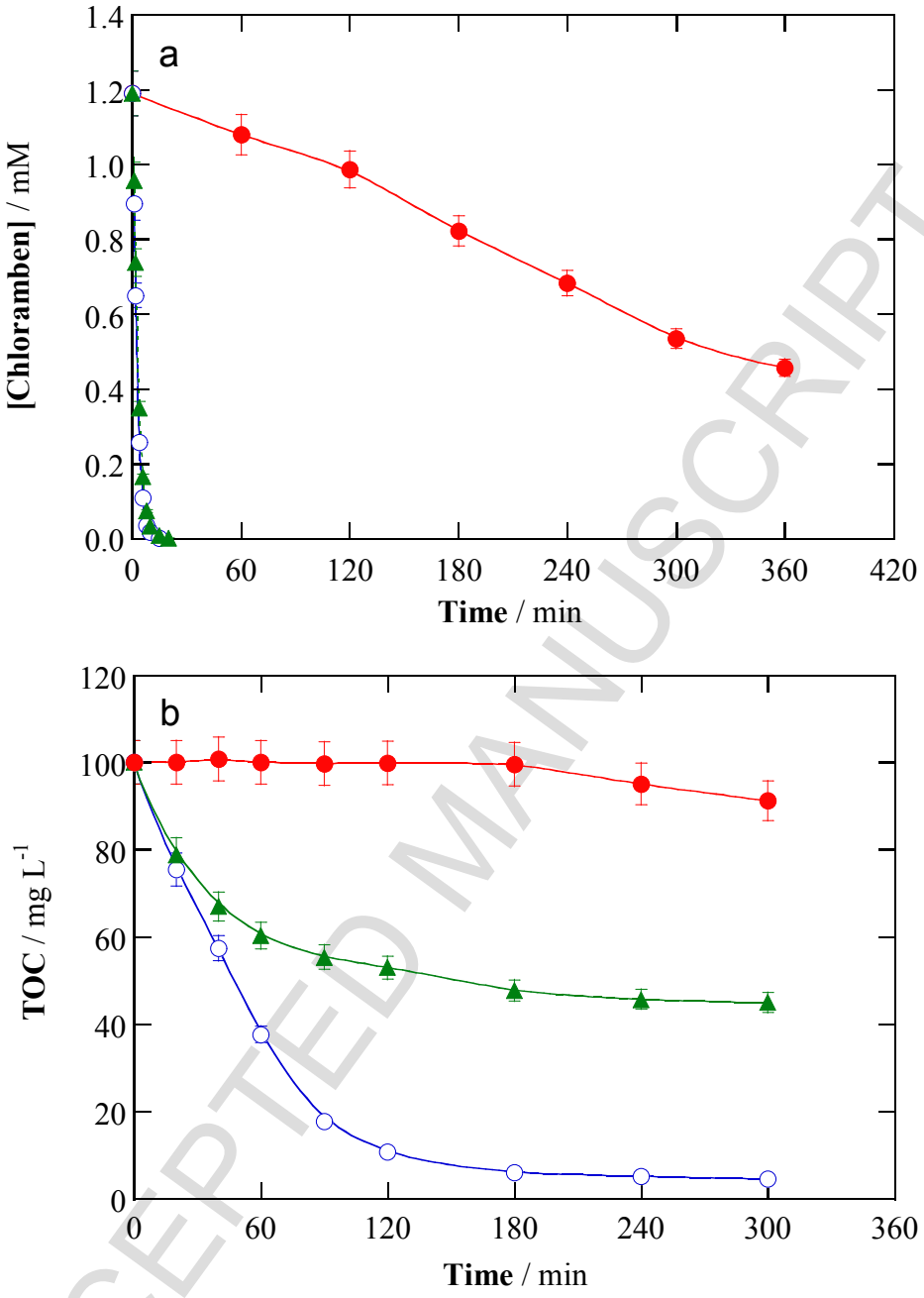

Fig. 2. (a) Herbicide concentration and (b) TOC vs. electrolysis time for the treatment of 100 mL of 1.19 mM chloramben in 0.050 M Na_2SO_4 at natural pH 3.42 using a stirred IrO_2-based/air-diffusion cell at j = 100 mA cm^{-2} and 35 °C. Method: (●) EO-H_2O_2, (▲) EF with 0.50 mM Fe^{2+} and (○) PEF with 0.50 mM Fe^{2+} and a 6 W UVA lamp.

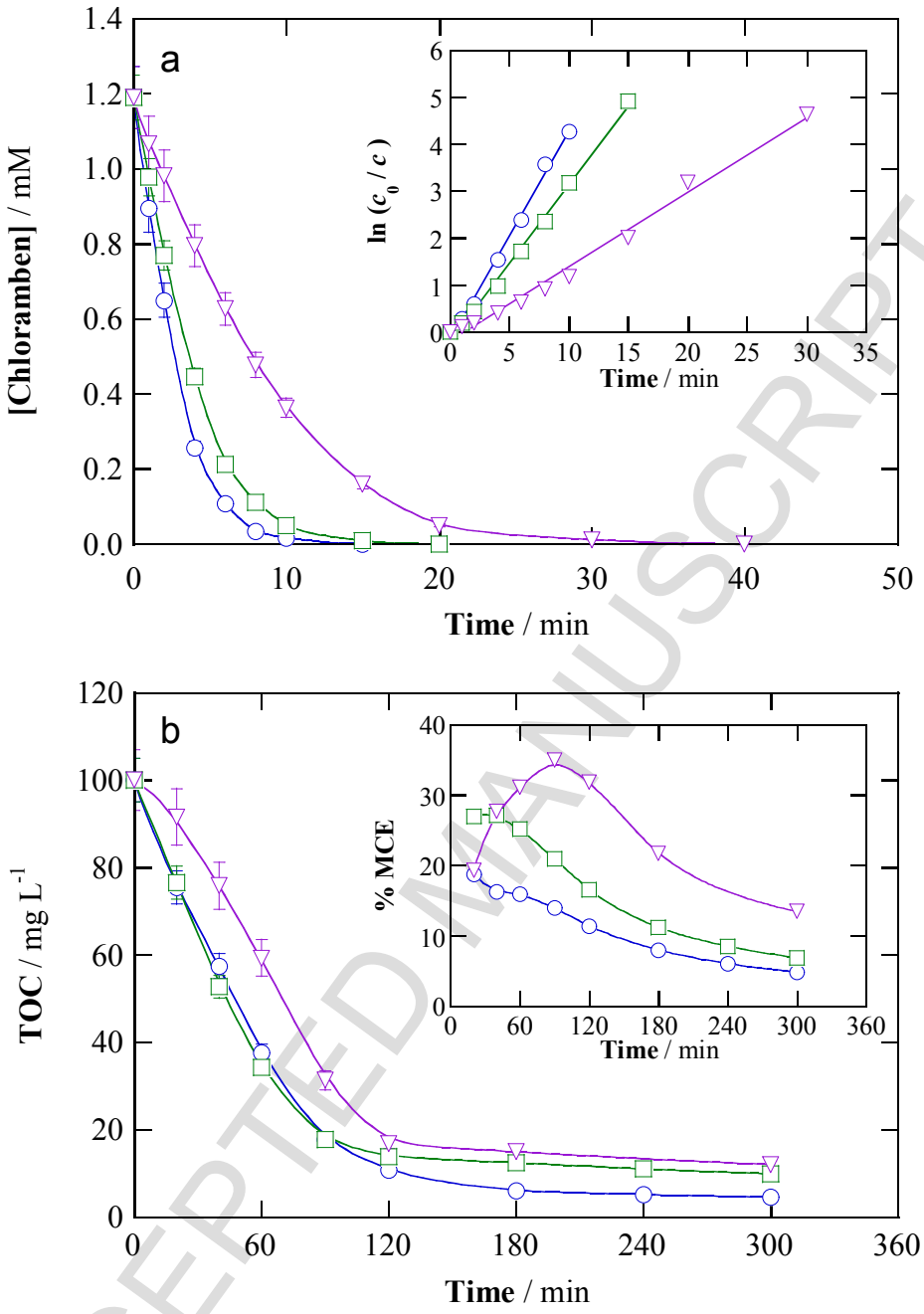

Fig. 3. Effect of current density on the change of (a) chloramben content and (b) TOC with electrolysis time for the PEF treatment of 100 mL of a 1.19 mM herbicide solution in 0.050 M Na_2SO_4 with 0.50 mM Fe^{2+} at natural pH 3.42 and 35 ºC, using a stirred IrO_2-based/air-diffusion cell. Current density: (○) 100 mA cm^{-2}, (□) 66.7 mA cm^{-2} and (▽) 33.3 mA cm^{-2}. The inset panels show the corresponding kinetic analysis for a pseudo-first-order reaction and MCE variation in (a) and (b), respectively.

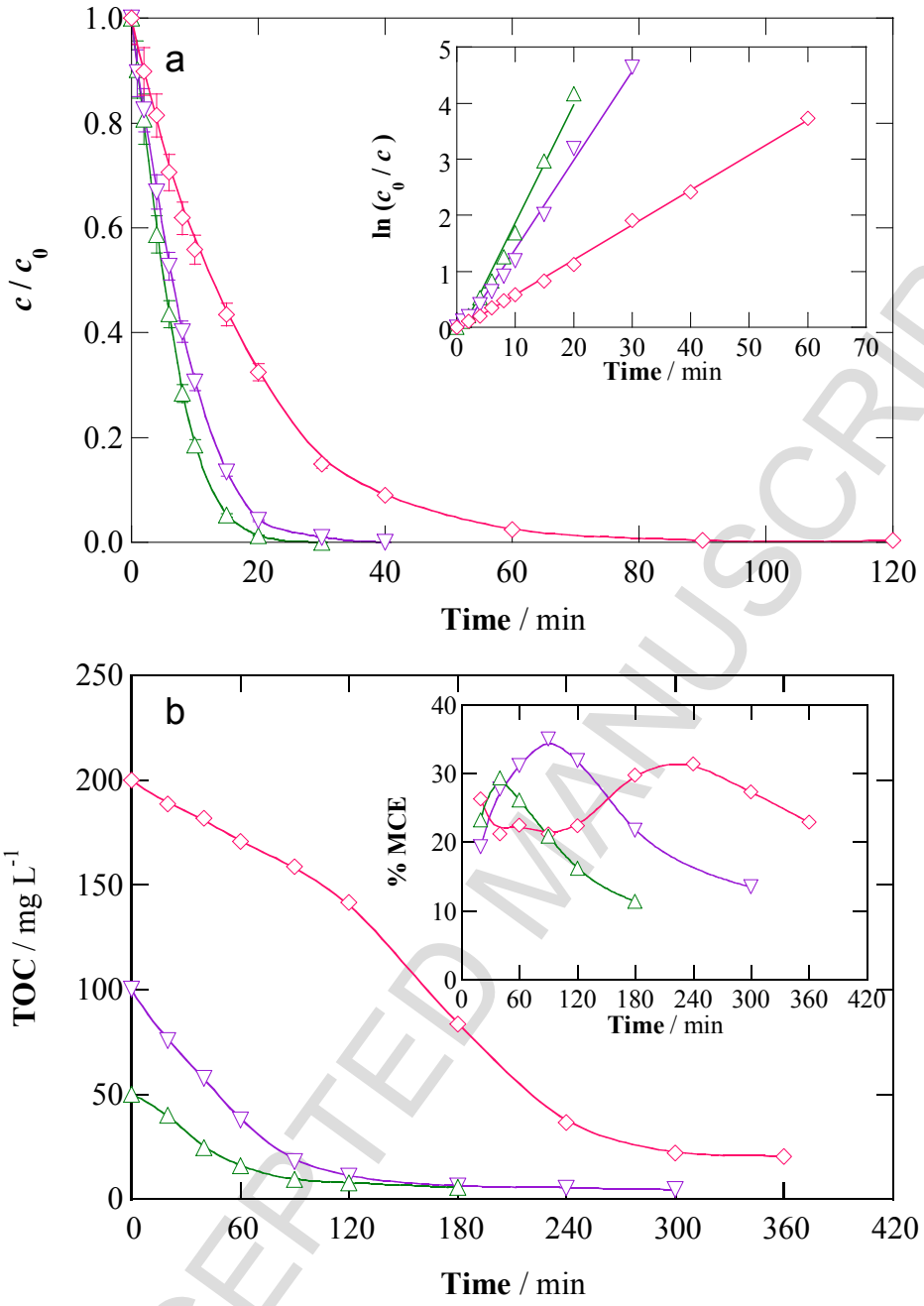

Fig. 4. Effect of herbicide concentration on (a) normalized chloramben content and (b) TOC abatement for the PEF degradation of 100 mL of herbicide solutions in 0.05 M Na_2SO_4 with 0.50 mM Fe^{2+} of natural pH using a stirred IrO_2-based/air-diffusion cell at j = 33.3 mA cm^{-2} and 35 ºC. $[Chloramben]_0$: (◇) 2.38 mM, (▽) 1.19 mM, and (△) 0.59 mM. The kinetic analysis for the herbicide removal and the change of MCE are presented in the inset panels of (a) and (b), respectively.

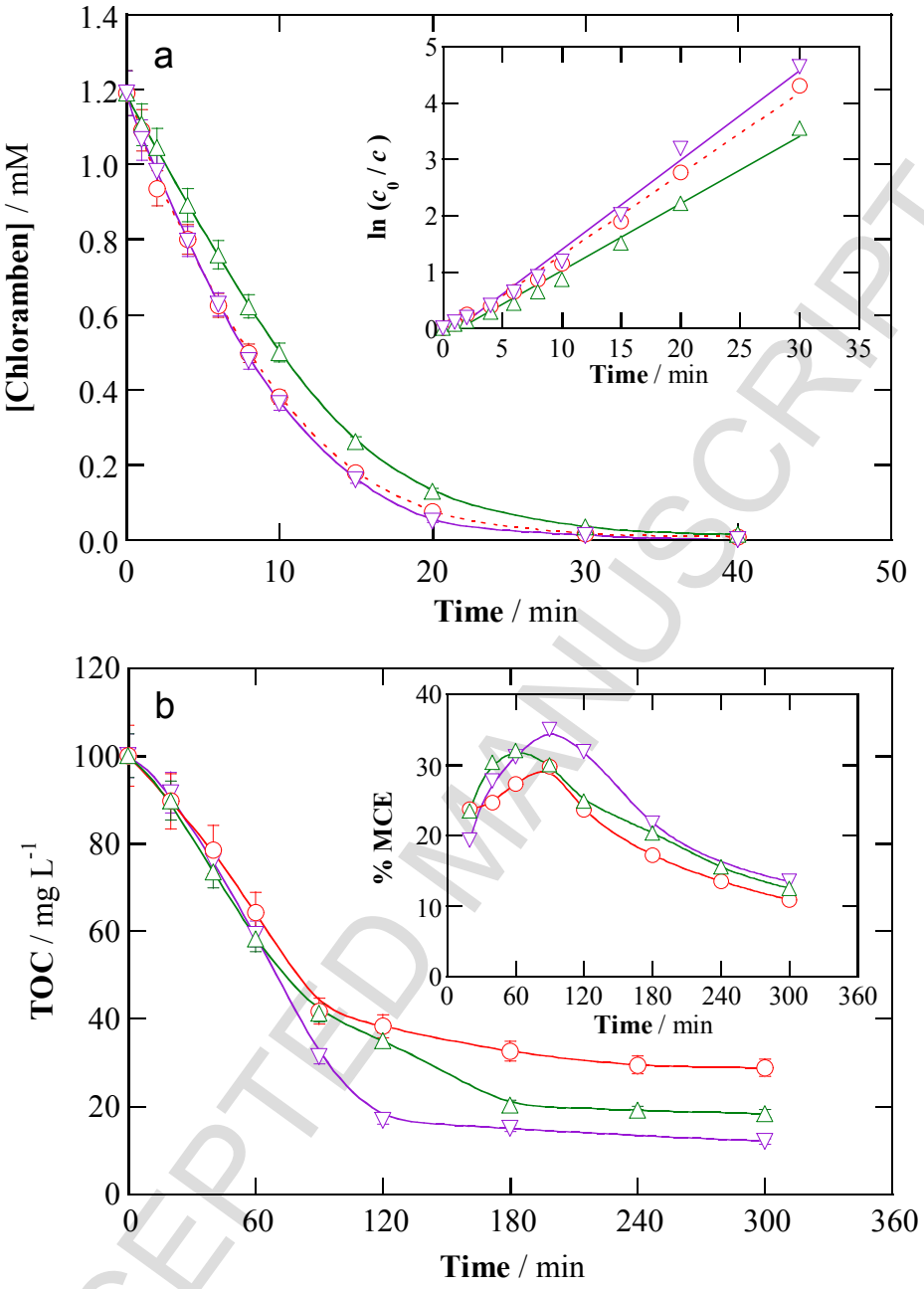

Fig. 5. Influence of chloride content on the variation of (a) chloramben concentration and (b) TOC with electrolysis time for the PEF treatment of 100 mL of 1.19 mM herbicide solutions with 0.50 mM Fe^{2+} at pH 3.4 using a stirred IrO_2-based/air-diffusion cell at j = 33.3 mA cm^{-2} and 35 ºC. Electrolyte composition: (▽) 0.050 M Na_2SO_4, (○) 0.035 M NaCl + 0.025 M Na_2SO_4 and (△) 0.011 M NaCl + 0.0015 M Na_2SO_4. The inset panels of (a) and (b) depict the corresponding pseudo-first-order kinetic analysis and the MCE values, respectively.

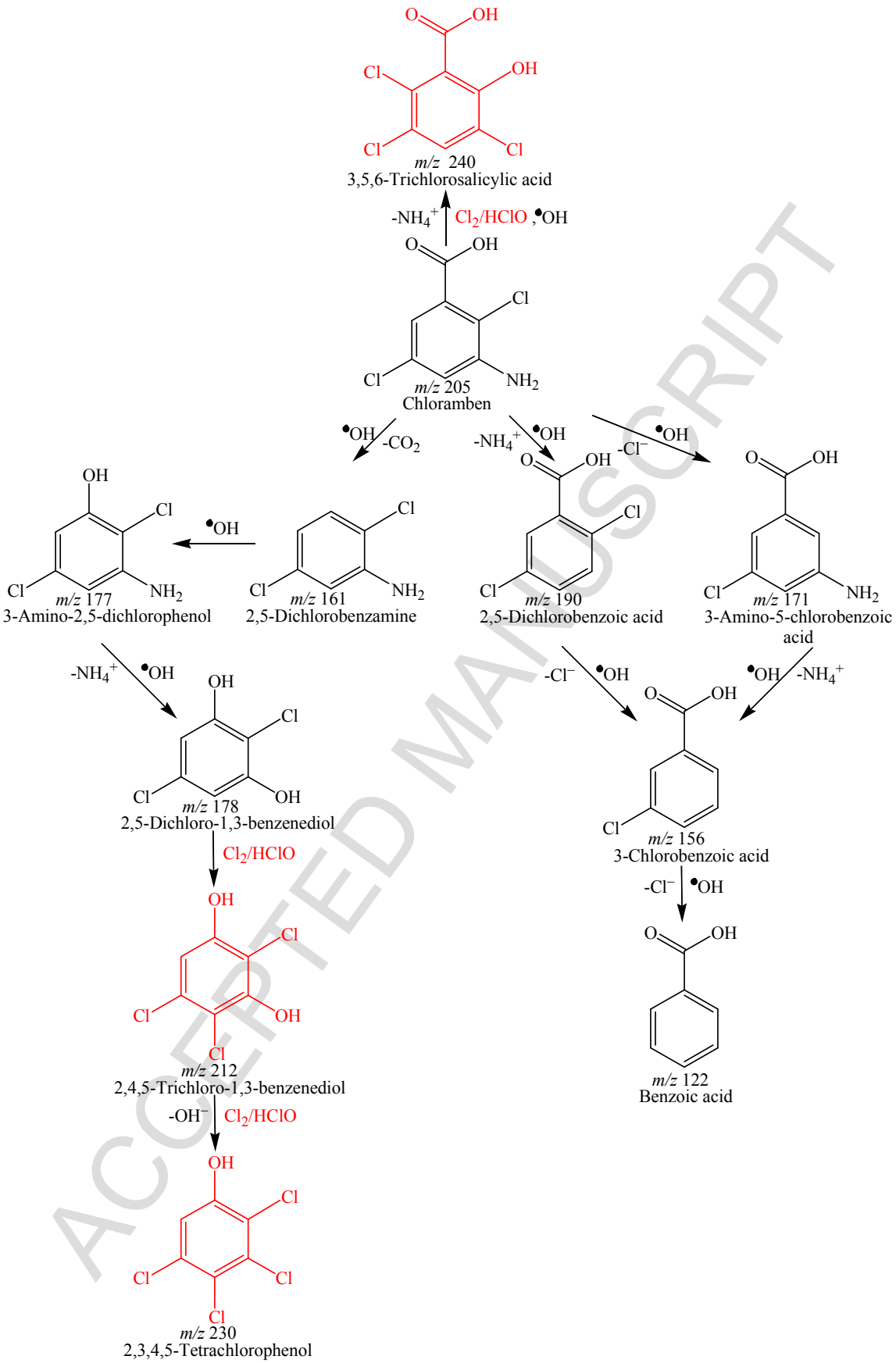

Fig. 6. Reaction sequence for initial chloramben degradation by PEF in sulfate and/or chloride medium.

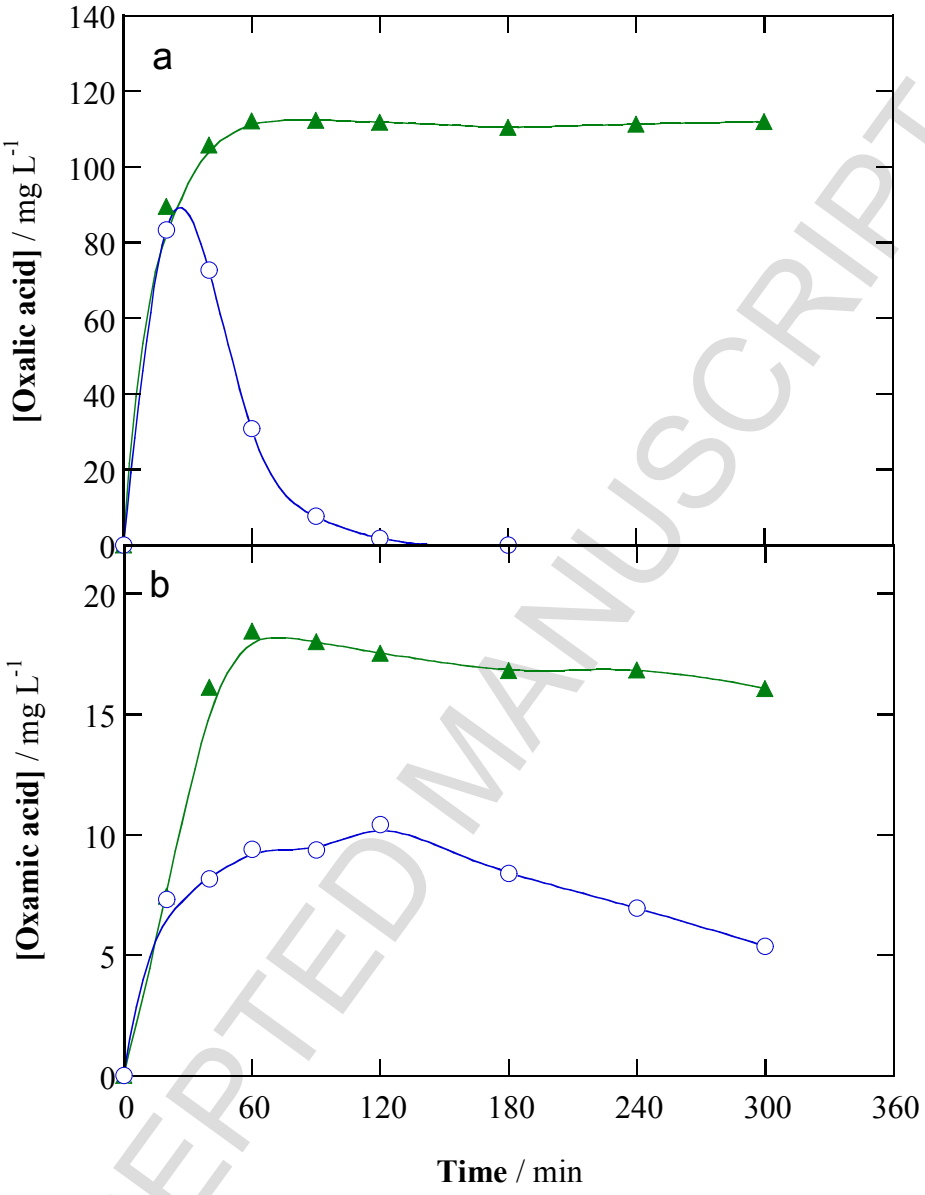

Fig. 7. Evolution of the concentration of (a) oxalic and (b) oxamic acids detected by ion-exclusion HPLC under the same conditions of the trials shown in Fig. 2 for (▲) EF and (○) PEF.

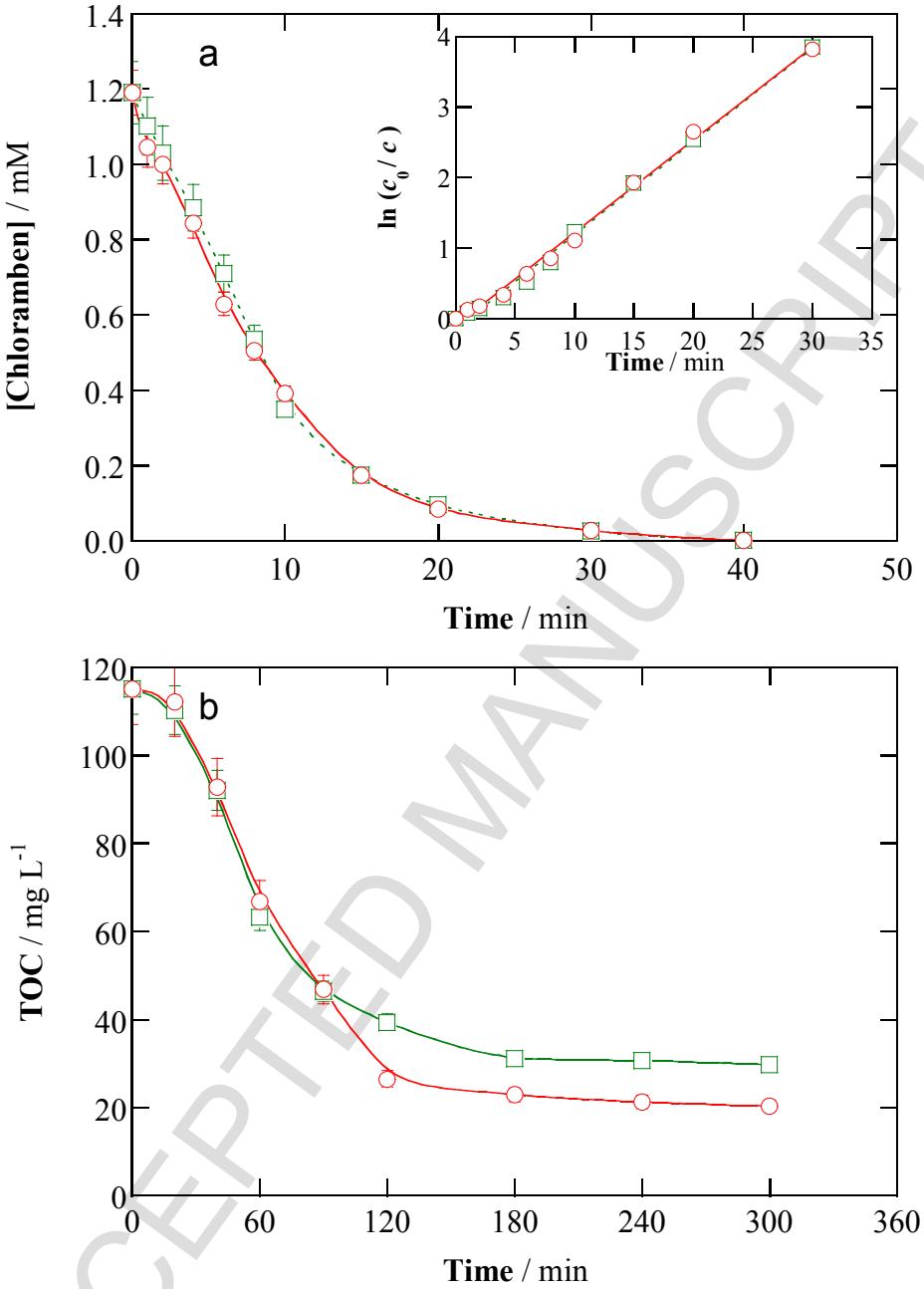

Fig. 8. Change of (a) herbicide concentration and (b) TOC with electrolysis time for PEF treatment of 100 mL of urban wastewater containing 1.19 mM chloramben and 0.50 mM Fe^{2+} at pH 3.4 using cells with an air-diffusion cathode and a (○) BBD or (□) IrO_2-based anode, operating at j = 33.3 mA cm^{-2} and 35 °C. In (a), the inset panel shows the kinetic analysis assuming a pseudo-first-order reaction.

Research highlights

▶ Fast and total removal of herbicide chloramben by PEF, not requiring pH regulation

▶ Performance of low cost IrO_2-based DSA® similar to that of expensive BDD

▶ Superiority of homogeneous $^{\bullet}OH$ over IrO_2($^{\bullet}OH$), BDD($^{\bullet}OH$), PbO_2($^{\bullet}OH$) and RuO_2($^{\bullet}OH$)

▶ Good performance of PEF in urban wastewater spiked with chloramben thanks to UVA light

▶ Chlorinated and/or non-chlorinated by-products identified in sulfate and chloride matrices.